J. Am. Chem. Soc. **1990**, *112*, 2892–2900

UV Resonance Raman Saturation Spectroscopy of Tryptophan Derivatives: Photophysical Relaxation Measurements with Vibrational Band Resolution

Junji Teraoka,† Paul A. Harmon, and Sanford A. Asher*

Contribution from the Department of Chemistry, University of Pittsburgh, Pittsburgh, Pennsylvania 15260. *Received June 5, 1989*

Abstract: We have developed a new technique to monitor photophysical relaxation processes with the resolution inherent in vibrational Raman scattering. We examine the ground-state ultraviolet resonance Raman saturation behavior of tryptophan derivatives excited in their S_3, S_2, and S_1 excited states in a well-defined, low laser pulse energy flux regime where multiphoton absorption is negligible and no Raman scattering is observed from photon-induced species. We derive a model for Raman saturation in this pulse energy flux regime which quantitatively relates the Raman saturation behavior to the absorption cross section and to the excited state relaxation rates. We detect novel differences in internal conversion efficiencies from the higher excited states of several tryptophan derivatives. We discuss specific applications of this new technique for the study of aromatic amino acid residue environments in proteins.

The sensitivity of molecular excited state relaxation rates to molecular microenvironment has motivated the development of numerous fluorescence methodologies.[1] The fact that the intrinsic fluorescence from many biological molecules is generally dominated by tryptophan emission has led to the extensive use of both time-resolved and steady-state tryptophan fluorescence as a probe of protein and enzyme structure and conformational dynamics.[2,3] Conformational and environmental changes are often accompanied by significant tryptophan fluorescence intensity changes associated with specific quenching interactions. There are, however, a few drawbacks in applying fluorescence techniques to large biological molecules. In the case of a system with a single tryptophan residue, the data analysis is, in principle, straightforward, but for multiple tryptophans, the residue fluorescence overlaps to prevent the acquisition of individual residue specific information. Additionally, fluorescence methodologies are generally not amenable to study the decay characteristics of the other aromatic amino acids, tryosine (tyr) and phenylalanine (phe), which show low fluorescence quantum yields when incorporated into polypeptides and proteins.[2,4] The prospect of examining tyr and phe fluorescence with deeper UV excitation, where these chromophores strongly absorb, appears unlikely due to the breadth and resulting overlap of tyr (maximum ca. 300 nm) and phe (maximum ca. 280 nm), as well as tryptophan (maximum ca. 340 nm) emission bands. The inability of fluorescence methodologies to study tyr and phe emission is unfortunate as these residues could provide two additional probes of protein structure.

The recent development of ultraviolet resonance Raman spectroscopy (UVRR) has been partially motivated by its potential utility for probing aromatic amino acid environments in proteins.[5,6] Previous UVRR studies have demonstrated the ability to selectively excite and resolve individual Raman bands of all three of the aromatic amino acids in proteins.[7-10] It appears possible to even distinguish between environmentally different amino acids by stepwise deuteration difference spectral techniques.[11] Typically, UVRR measurements probe changes in aromatic amino acid environment by monitoring vibrational frequency shifts and/or changes in Raman cross sections. The frequency shifts would derive from alterations in interresidue interactions such as hydrogen bonding, while cross-section changes would derive from alterations in the resonant and preresonant electronic transitions, hypochromic interactions, and changes in the chromophore local refractive index. It would be expected that UVRR band frequencies and cross sections might also be sensitive to excited-state relaxation rates, but unfortunately this is not generally realized because the resonant electronic transitions are often dominated by inhomogeneous broadening in condensed-phase systems. Indeed, in most UVRR applications, excitation occurs in upper singlet excited states in order to avoid fluorescence interference. The relaxation rates from these levels are dominated by intramolecular (intraresidue) processes and are thus insensitive to the molecular microenvironment.

We demonstrate here the use of a new Raman spectroscopic technique which probes excited-state relaxation rates with the vibrational resolution inherent in Raman measurements. We carefully examine the nonlinear dependence of UVRR intensities upon the laser pulse energy flux. This nonlinear behavior, or "saturation", reflects ground-state depletion of the analyte species during the laser pulse. The degree of ground-state depletion is a function of the rates of both excited-state population (via optical absorption) and relaxation during the laser pulse. Although a few previous studies have also examined nonlinearities in UVRR measurements,[12-14] these studies only qualitatively modeled ground-state saturation and did not relate the saturation to excited-state population and relaxation. In addition, two of these previous studies[12,13] examined these phenomena at photon fluxes ca. 30-fold larger than reported here, in a regime where photon-driven relaxations (*vide infra*) and excited-state absorption mask the first-order excited-state relaxation processes.

In this work we examine the saturation of ground-state resonance Raman vibrational intensities over a low pulse energy flux regime. We demonstrate that in this flux regime the saturation behavior can be quantitatively related to excited-state population relaxation rates occurring during nanosecond laser pulse excitation.

* Author to whom correspondence should be addressed.
† Present address: Osaka City University, Osaka, Japan.

(1) See for example: Lakowicz, J. R. *Principles of Fluorescence Spectroscopy*; Plenum Press: New York, 1983.
(2) Longworth, J. W. In *Time Resolved Fluorescence Spectroscopy in Biochemistry and Biology*; Cundall, R. B., Dale, R. E., Eds.; Plenum: London, 1983.
(3) Beechem, J. M.; Brand, L. *Annu. Rev. Biochem.* **1985**, *54*, 43.
(4) Longworth, J. W. In *Excited States of Proteins and Nucleic Acids*; Steiner, R. F., Weinryb, I., Eds.; Plenum: New York, 1971; pp 319–484.
(5) See for example: Asher, S. A. *Annu. Rev. Phys. Chem.* **1988**, *39*, 537 and references therein.
(6) Harada, I.; Takeuchi, H. *Spectroscopy of Biological Systems*; Clark, R. J., Hestor, R. E., Eds.; John Wiley and Sons: New York, 1986; Chapter 3.
(7) Rava, R. P.; Spiro, T. G. *J. Phys. Chem.* **1985**, *89*, 1856.
(8) Asher, S. A.; Ludwig, M.; Johnson, C. R. *J. Am. Chem. Soc.* **1986**, *108*, 3186.
(9) Rava, R. P.; Spiro, T. G. *Biochemistry* **1985**, *24*, 1861.
(10) Copeland, R. A.; Spiro, T. G. *Biochemistry* **1985**, *24*, 4960.
(11) Miura, T.; Takeuchi, H.; Harada, I. *Biochemistry* **1988**, *27*, 88.
(12) Johnson, C. R.; Ludwig, M.; Asher, S. A. *J. Am. Chem. Soc.* **1986**, *108*, 905.
(13) Bajdor, K.; Nishimura, Y.; Peticolas, W. L. *J. Am. Chem. Soc.* **1987**, *109*, 3514.
(14) Ludwig, M.; Asher, S. A. *J. Am. Chem. Soc.* **1988**, *110*, 1005.

0002-7863/90/1512-2892$02.50/0

Table I

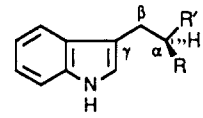

I compd	II[a] R	III[a] R'	IV[b] S_1/S_2 lifetime components (ns) A, %	τ_1	τ_2	V[c] single population weighted phenomenological lifetime (ns)	VI[d] best fit value for $(1/K)$, eq 8, Raman data S_1/S_2 excitation (ns)	VII[e] best fit value for $(1/K)$, eq 8, Raman data S_3 excitation (ns)
TRP	NH_3^+	CO_2^-	22	0.62	3.2	2.2	2.4 ± 0.3	>15
NATA	$NHCOCH_3$	$CONH_2$	100	3		3		2.9 ± 0.5
NATA (quenched with NaI)	$NHCOCH_3$	$CONH_2$	100	0.65		0.65	0.75 ± .05	
NATE	$NHCOCH_3$	$CO_2C_2H_5$	32	0.42	1.70	1.1		1.3 ± 0.2
TRPAM (pH 5)	NH_3^+	$CONH_2$	54	1.14	2.0	1.4	1.5 ± 0.1	3.5 ± 0.2
TRPAM (pH 9)	NH_2	$CONH_2$	100	7		7	7.2 ± 1.5	7.1 ± 1.4

[a] Columns II and III show the R and R' substituent groups for the species listed in column I. [b] Column IV gives the percentage of the population exhibiting the S_1/S_2 lifetime τ_1, the remainder of the population has the lifetime described by τ_2 (data from Petrich et al.).[17] [c] Column V lists the phenomenological single lifetime value which is obtained from eq 8 given the relaxation components listed in column IV. [d] Column VI gives the average best fit values of $(1/K)$ to the 1578 and 1622 cm^{-1} Raman saturation data for S_1/S_2 excitation. [e] Column VII lists the average value of $1/K$ derived from the 760, 1015, and 1555 cm^{-1} saturation data excited in S_3.

This provides a methodology to monitor photophysical relaxation processes with the vibrational resolution inherent in Raman measurements. We call this new spectroscopic technique UV resonance Raman saturation spectroscopy.[15] We examine the Raman saturation behavior of a series of tryptophan derivatives with essentially identical electronic transitions, but which have widely varying nonradiative relaxation rates from their lowest excited singlet states. These compounds were selected because their radiative and nonradiative rates have previously been well characterized by time-resolved fluorescence techniques.[16-22] Thus, these compounds provide quantitative tests for our UV Raman saturation model. Further, the photophysics of tryptophan remains of considerable interest, and certain aspects of its photophysics, particularly the mechanism for photoionization from higher singlet excited states,[23-28] remains unclear. The major motivation for the present study is that the study of tryptophan derivative saturation is a logical first step for studying tyrosine, phenylalanine, and tryptophan residue excited-state relaxation rates in proteins, as probes of amino acid residue environments and protein conformation.

Our UV saturation results are analyzed in the context of the known tryptophan-derivative excited-state relaxation rates. We present a simple model which quantitatively describes the saturation behavior in terms of absorption cross sections, laser pulse energy fluxes, and excited-state lifetimes. Our saturation data also reveal novel differences in internal conversion efficiencies for several derivatives, which involves the presence of a protonated amino group near to the indole ring. In a subsequent report we will describe the utilization of UV resonance Raman saturation spectroscopy to study aromatic amino acids in proteins.

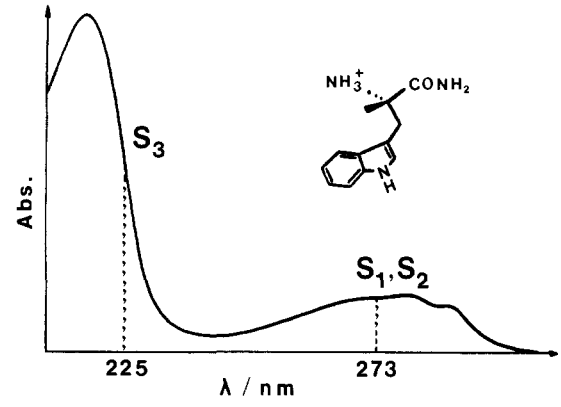

Figure 1. UV absorption spectrum of an aqueous solution of tryptophanamide (TRPAM, pH 5).

Experimental Section

L-Tryptophan (TRP), *N*-acetyl-L-tryptophanamide (NATA), L-tryptophanamide (TRPAM), and *N*-acetyl-L-tryptophan ethyl ester (NATE) were obtained from Sigma Chemical Co. and used without further purification. The instrumentation used to obtain the UVRR spectra has been described in detail elsewhere.[29] The Nd-Yag based system generates 20-Hz UV pulses with pulse widths of ca. 4 ns. The Raman scattered light was collected in a backscattering geometry. The ca. 20-mL samples were pumped rapidly through a dye laser jet nozzle and recirculated during the 5–10 min Raman measurement. The flow rate was sufficient to supply fresh sample to the illuminated sample volume between laser pulses. The excitation beam was focused 2 cm beyond the sample with a 25 cm focal length lens. The beam was positioned at a point where the sample thickness is estimated to be 150–200 μm at ca. 1 mm from the jet nozzle tip. The spot size and intensity distribution of the excitation beam at the front face of the sample were measured by translating a razor blade mounted on a micrometer stage across the beam and monitoring the transmitted power. Typical laser beam spot sizes at the samples were ca. 1 mm^2. The pulse energy was measured by using a Scientech Model 361 power meter. Pulse energies were attenuated by placing Suprasil neutral density filters (Melles Griot) in the beampath.

The TRP derivative concentrations were ca. 3 mM for the 273 nm excitation studies and 0.5–1 mM for the 225 nm excitation studies. This gave absorbances of ca. 0.3 through the jet sample thickness. $NaClO_4$ (1.0 M) was used as a non-absorbing internal Raman intensity standard. Small adjustments of the analyte concentrations were made so that the absorbance at the excitation frequency was kept identical in all cases. This ensures identical exponential decreases in the laser intensity between samples as the beam transmits through the imaged sample volume. This

(15) Teraoka, J.; Harmon, P. A.; Asher, S. A. *Proc. Int. Conf. Raman Spectrosc., 11th* **1988**, 547.
(16) Wijnaedts Van Resandt, R. W. *Chem. Phys. Lett.* **1983**, *95*, 205.
(17) Petrich, J. W.; Chang, M. C.; McDonald, D. B.; Fleming, G. R. *J. Am. Chem. Soc.* **1983**, *105*, 3824.
(18) Chang, M. C.; Petrich, J. W.; McDonald, D. B.; Fleming, G. R. *J. Am. Chem. Soc.* **1983**, *105*, 3819.
(19) Szabo, A. G.; Rayner, D. M. *J. Am. Chem. Soc.* **1980**, *102*, 554.
(20) Engh, R. A.; Chen, Lin X.-Q.; Fleming, G. R. *Chem. Phys. Lett.* **1986**, *126*, 365.
(21) For a review, see: Creed, D. *Photochem. Photobiol.* **1984**, *39*, 537.
(22) Robbins, R. J.; Fleming, G. R.; Beddard, G. S.; Robinson, G. W.; Thistlewaite, P. J.; Woolfe, G. J. *J. Am. Chem. Soc.* **1980**, *102*, 627.
(23) Amouyal, E.; Bernas, A.; Grand, D. *Photochem. Photobiol.* **1979**, *29*, 1071.
(24) Steen, H. B. *J. Chem. Phys.* **1974**, *61*, 3997.
(25) Tatischeff, I.; Klein, R. *Photochem. Photobiol.* **1975**, *22*, 221.
(26) Steen, H. B.; Bowman, M. K.; Kevan, L. *J. Phys. Chem.* **1976**, *80*, 482.
(27) Steen, H. B.; Konshaug, M. In *Proceedings of the International Conference on Excited States of Biological Molecules*; Birks, J. B., Ed.; Wiley: New York, 1976.
(28) Ottolenghi, M. *Chem. Phys. Lett.* **1971**, *12*, 339.
(29) Asher, S. A.; Johnson, C. R.; Murtaugh, J. *Rev. Sci. Instrumen.* **1983**, *54*, 1657.

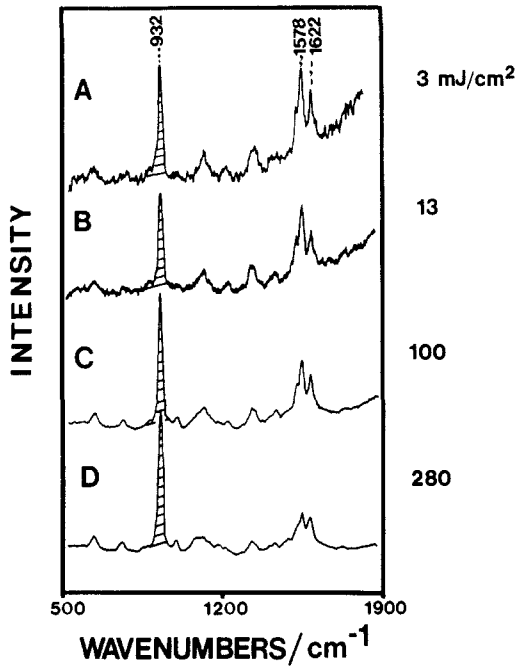

Figure 2. Resonance Raman spectra of tryptophanamide (TRPAM, pH 9) excited at 273 nm obtained with increasing pulse energy flux. Pulse energy fluxes are listed on the right in units of mJ/cm². The internal standard perchlorate band at 932 cm⁻¹ is shaded. Note the decreases in the relative intensity ratios of the TRPAM bands with higher energy fluxes.

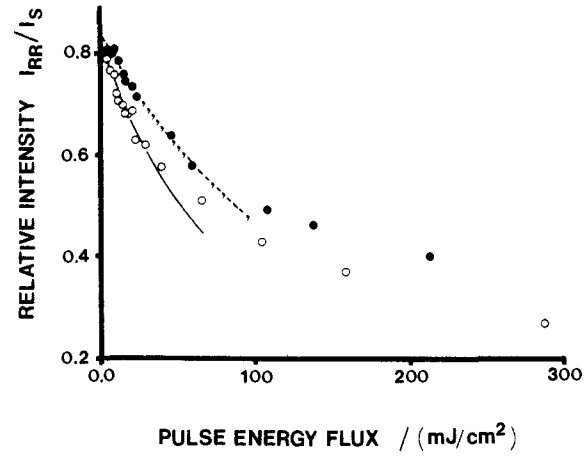

Figure 3. Saturation of the relative intensity ratio of the tryptophanamide (TRPAM) 1578-cm⁻¹ band to the 932-cm⁻¹ internal standard band as a function of pulse energy flux. TRPAM 3 mM, perchlorate 1 M: (○) TRPAM (pH 9); (●) with 0.5 M sodium iodide added. The solid and dashed curves are discussed in the text.

was verified by monitoring the absolute perchlorate Raman intensities as a function of laser energy flux for each of the TRP derivative saturation studies. We observed identical ClO_4^- intensities for each TRP derivative with identical incident pulse energy fluxes. The ClO_4^- intensities increased linearly with increasing laser energy flux, indicating no significant bleaching of the TRP derivative absorption along the laser beam path.

The relative intensity ratios used for our calculations derived from peak height measurements. No changes in bandshapes were observed over the flux regimes studied here. No permanent loss of analyte was observed during the 5–10 min scan times. Further, we only illuminate 5–10% of the total sample volume in this time and replace the sample between scans.

Results

S_1/S_2 Excitation. Figure 1 shows the absorption spectra of L-tryptophanamide (TRPAM) (pH 5) in aqueous solution. The absorption spectra of all of the tryptophan derivatives are very similar and show the same absorption bands with similar relative intensities (±20%) and band maxima. The molecular structure of TRPAM (pH 5) is also shown as are the electronic transitions and the excitation wavelengths used. Table I shows the substitution pattern for the other tryptophan derivatives studied here. Figure 2 shows four representative resonance Raman spectra of L-tryptophanamide (TRPAM) at pH 9 obtained with increasing pulse energy flux. The spectra were excited at 273 nm in resonance with the ^1L_b, $^1L_a \leftarrow {}^1A$ π–π^* singlet electronic transition of the indole moiety, which we will refer to as S_1/S_2. The 1622 and 1578 cm⁻¹ ν_{8a} and ν_{8b} benzene-like indole vibrations are selectively enhanced because they vibronically mix with strong higher energy indole electronic transitions.[6] The spectra in Figure 2 demonstrate that the Raman intensities of the TRPAM bands decrease relative to the internal standard band (shaded) as the energy flux increases. The open circles in Figure 3 show the energy flux dependence of the ratio of the TRPAM (pH 9) 1578-cm⁻¹ Raman band intensity relative to that of the ClO_4^- internal intensity standard band. The decreasing relative intensity ratio simply reflects the decreasing number of TRPAM ground-state species (integrated over the laser pulse) in the imaged sample volume that are available for Raman scattering as the pulse energy flux increases. The initial rate of decrease of the TRPAM (pH 9) relative intensity ratio begins to level off at ca. 30 mJ/cm². The solid line in Figure 3 was calculated from a photophysical model (vide infra) which was fit to the 0–30 mJ/cm² data which utilizes only the known radiative and nonradiative relaxation rates from S_1/S_2 states. Although the model easily fits the 0–30 mJ/cm² pulse energy flux data, the model underestimates the relative intensity ratio at higher energy fluxes. Apparently, recovery of the ground state is augmented by some photon driven process which begins to turn on at ca. 30 mJ/cm² under our experimental conditions. This additional photon driven process dominates the saturation behavior between 30 and 250 mJ/cm² and causes the 1578-cm⁻¹ band to ClO_4^- band intensity ratio to become only weakly dependent upon the pulse energy flux. In fact, the behavior is rather insidious in the high energy flux regions, where the analyte and the internal standard Raman intensity increase together almost linearly with laser power. However, the intensity ratio is artificially low and any Raman cross section determined from this observed relative ratio will be more than 2-fold smaller than its true value.

The solid circles in Figure 3 show a similar saturation curve for a TRPAM (pH 9) solution containing 0.5 M sodium iodide. Iodide is a commonly used collisional fluorescence quencher that increases the $S_1/S_2 \rightarrow S_0$ nonradiative rate. These data initially show a less steep energy flux saturation slope than was observed for unquenched TRPAM. The dashed curve is a fit for the 0–30 mJ/cm² data using the same model used for the unquenched TRPAM. In this case, the model successfully describes the observed data until ca. 85 mJ/cm² where the calculated relative ratios are again less than those observed, which again indicates an enhanced ground-state recovery rate. We find that all the TRP analogues excited in the S_1/S_2 transition exhibit a behavior where an additional ground-state recovery process becomes active at high pulse energies. The energy flux threshold for this additional recovery process increases as the S_1/S_2 lifetime decreases. Although interesting in its own right, this photon-induced relaxation limits the energy flux range over which we can acquire data dominated by the normal well-known radiative and nonradiative processes from S_1/S_2.

Figure 4 shows the saturation behavior for S_1/S_2 excitation for several TRP derivatives at energy fluxes below where this photon driven relaxation is observed. The data have been corrected for concentration differences arising from our requirement that the absorbance of each sample be identical at the excitation frequency. Shown in Figure 4 is *N*-acetyl-L-tryptophanamide (NATA) quenched with 0.5 M NaI, TRPAM (pH 5), L-tryptophan (TRP), and TRPAM (pH 9) data from Figure 3. NATA was quenched to give a wider range of S_1/S_2 lifetimes for our study. The S_1/S_2 lifetime of NATA as a function of added sodium iodide is known.[16] The relative S_1/S_2 lifetimes of these compounds are the following: NATA quenched with 0.5 M NaI < TRPAM (pH 5) < TRP < TRPAM (pH 9) (vide infra). We expect that a longer lived S_1/S_2

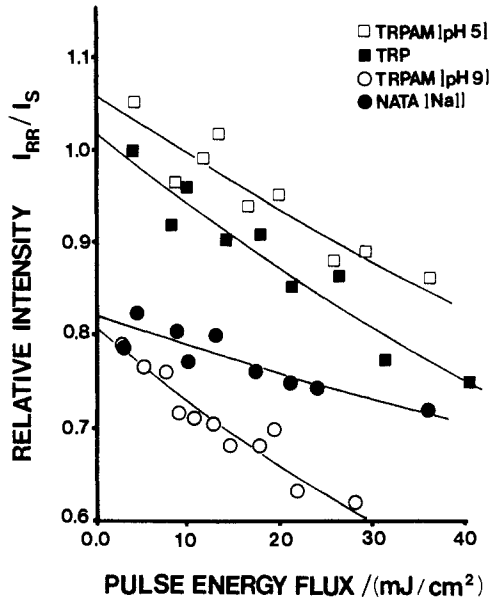

Figure 4. Saturation of the 1578-cm^{-1} band of TRP (solid squares), TRPAM (pH 5) (open squares), NATA quenched with 0.5 M NaI (solid circles), and TRPAM (pH 9) (open circles). Note the lower flux energy regime compared to Figure 3. TRP derivative concentration is 3 mM. 1 M perchlorate, 273-nm excitation.

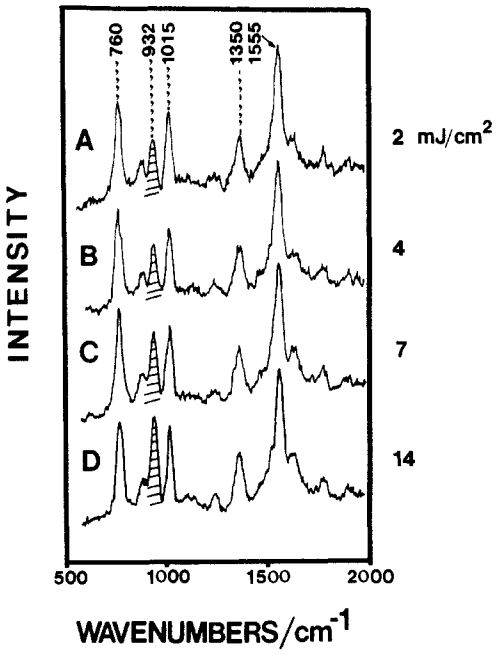

Figure 5. Resonance Raman spectra of TRP (pH 6.5) excited at 225 nm with pulse energy fluxes below 15 mJ/cm^2. Pulse energy fluxes listed in units of mJ/cm^2. Internal standard band shaded.

excited state will result in more extensive ground-state depopulation and a more rapid decrease in the analyte to internal standard intensity ratio with increasing pulse energy flux. This is clearly observed in Figure 4. It should be noted that the different relative intensity ratios at zero energy flux reflect the intrinsically different Raman cross sections at 273-nm excitation for the 1578-cm^{-1} band for these TRP analogues.

S_3 Excitation. Excitation at 225 nm is in resonance with the allowed $^1B_b \leftarrow {}^1A$ electronic transition[30] of the indole ring which we denote as S_3. At 225 nm the molar absorptivities are ca. 20000–25000 M^{-1} cm^{-1}, which are 4- to 5-fold larger than at 273 nm. The 225-nm excited resonance Raman spectra of the TRP derivatives are dominated by the totally symmetric indole modes

(30) Song, P. S.; Kurtin, W. E. *Photochem. Photobiol.* **1969**, *9*, 175.

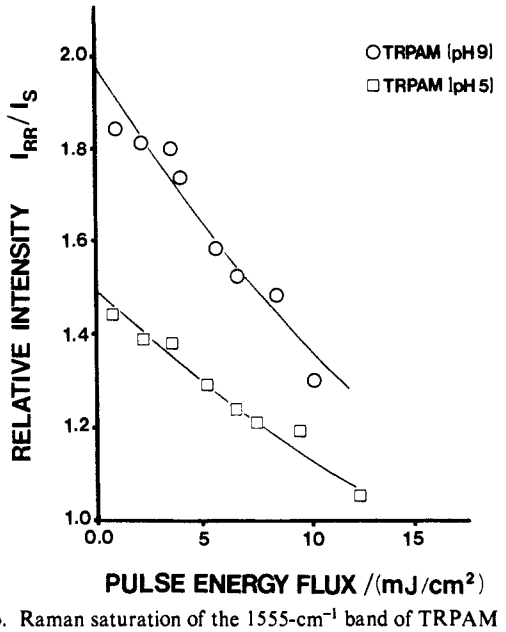

Figure 6. Raman saturation of the 1555-cm^{-1} band of TRPAM (pH 9) (open circles) and TRPAM (pH 5) (open squares) at 225-nm excitation. 0.5 mM analyte, 1 M perchlorate. Solid curves derive from a quantitative model for the saturation. See text for details.

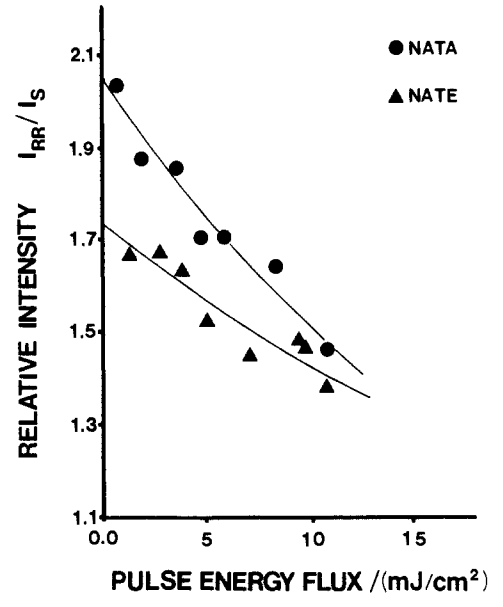

Figure 7. Raman saturation for NATA (circles) and NATE (triangles). 0.5 mM NATA and NATE, 1 M perchlorate.

at ca. 760, 1015, and 1555 cm^{-1} (Figure 5). As observed for S_1/S_2, we see decreases in the intensity ratio of the TRP derivative to the internal standard bands as the energy flux increases, and we also observe the onset of photon-driven relaxation at higher fluxes. Additionally, photochemical transient Raman bands which overlap the 760- and 1015-cm^{-1} ground-state bands begin to contribute to the spectra at high-energy fluxes. At high-energy fluxes the analyte to internal standard intensity ratio again becomes relatively independent of energy flux. Significant ground-state depopulation and Raman saturation occurs at pulse energies below ca. 15 mJ/cm^2, well before any transient Raman bands are observed. This is evident in Figure 5 which shows four 225-nm excited TRP (pH 6.5) resonance Raman spectra obtained with pulse energy fluxes below 15 mJ/cm^2. The TRP to internal standard relative intensity ratios change by about a factor of 2 over this energy flux region, which corresponds to a maximum average laser power of ca. 2 mW at a 20 Hz repetition rate focused to a 1 mm^2 spot size as described in the Experimental Section. Figures 6–8 show the 225-nm saturation curves for the 1555-cm^{-1} band for all the compounds studied in a low energy flux region

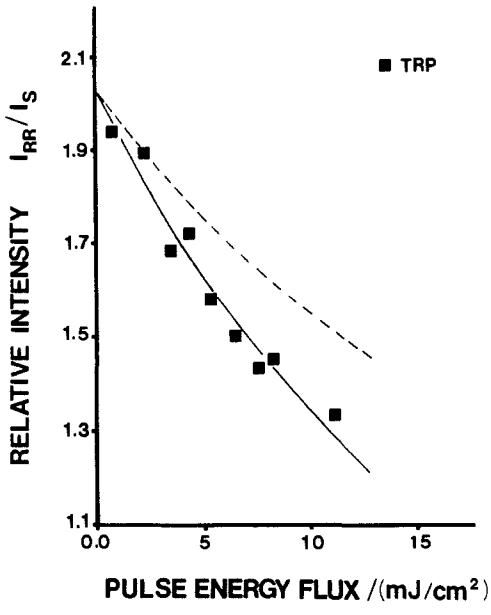

Figure 8. Raman saturation for the 1555-cm^{-1} band of TRP. Conditions as described in Figures 6 and 7.

where photochemical transient and photon induced relaxation contributions are absent. Other vibrational modes show similar behavior. The data in Figures 6–8 have been corrected for concentration differences. The different relative ratios at zero energy flux reflect the differing Raman cross sections for the 1555-cm^{-1} vibration for the different TRP derivatives. Since the normal mode character of the 1555-cm^{-1} band and the nature of the S_3 transition in all these derivatives is identical, Raman theory predicts that the Raman cross sections should be roughly proportional to the square of the molar absorptivities near 225 nm. Our results quantitatively agree with this expectation. In Figure 6, for example, the ratio of the TRPAM (pH 9)/TRPAM (pH 5) Raman cross sections is 0.76. The calculated relative molar absorptivity ratio at 225 of 0.87 is close to the 0.84 measured ratio.

Discussion

TRP S_1/S_2 Relaxation Mechanisms. Table I displays the structures and S_1/S_2 lifetimes of the TRP derivatives studied here as determined by Petrich et al.[17] using time-resolved fluorescence techniques. The NATA quenched with 0.5 M NaI fluorescence lifetime value derives from Wijnaendts Van Resandt.[16] The variation in the S_1/S_2 lifetimes has been successfully explained by Petrich et al.[17] and refined later by Engh et al.[20] and involves a modulation of the nonradiative $S_1/S_2 \rightarrow S_0$ rate by the R and R′ groups. The explanation utilizes three assumptions: (1) the R and R′ groups may charge transfer quench the excited indole ring to give ground-state indole; (2) the quenching efficiency depends on the electrophilicity of the R and R′ groups and their proximity to the indole ring; and (3) various possible rotational isomers about the α-β and the β-γ C–C bonds[20] (see notation indicated in Table I) define the proximity of R and R′ groups to the indole ring. Rotomers about the α–β bond may interconvert on the fluorescence time scale while rotomers about the β–γ bond cannot. The observed S_1/S_2 fluorescence lifetimes and decay (i.e. single or double exponential) can then be rationalized on the basis of the relative rotational isomer populations and group electrophilicities in the order $CO_2H > CO_2CH_2CH_3 > NH_3^+ > CONH_2 \cong NHCOCH_3 > CO_2^-, NH_2$. Compounds where R and R′ have similar electrophilicities (NATA), or where R and R′ combined are weakly electrophilic (TRPAM, pH 9), will exhibit single exponential decays. All other compounds will exhibit double exponential decays as seen in Table I.

The reciprocal of the fluorescence lifetimes displayed in Table I gives the sum of the radiative and nonradiative decay rates out of the thermalized S_1/S_2 fluorescing levels. A quantitative correlation between Raman saturation behavior and fluorescence lifetimes will only be possible if the rate of decay of molecules

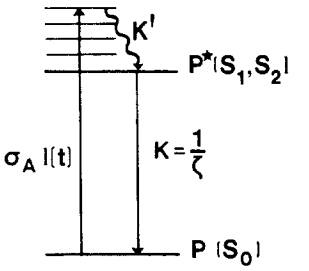

Figure 9. Model for Raman saturation for excitation in S_1/S_2 at 273 nm. See text for details.

from S_1/S_2 corresponds to the rate of repopulation of S_0 during the laser pulse. Decay from S_1/S_2 to states that are long lived relative to the laser pulse width must be minimal; this is the case for each of the compounds in Table I. The three processes that contribute to the S_1/S_2 decay rates are (1) charge-transfer quenching, (2) radiative decay, and (3) intersystem crossing. Photoionization from S_1/S_2 fluorescing levels is quite small (less than 1%).[23,31,32] Only intersystem crossing leads to the formation of long-lived states while charge-transfer quenching directly yields ground-state indole. Fluorescence emission yields ground electronic state species in higher vibrational levels of S_0 which thermalize on the picosecond time scale to a Boltzmann vibrational ground-state population. The radiative and intersystem crossing rates for the compounds in Table I are relatively independent of R and R′ and are ca. 6×10^7 and 3×10^7 s^{-1}, respectively.[18,22] The ca. 10-fold smaller intersystem crossing rate compared to the S_1/S_2 relaxation rate gives 5–10% triplet quantum yields for TRP, NATA, NATE, and TRPAM (pH 5) and shows that S_1/S_2 relaxation largely corresponds to repopulation of S_0.

Raman Saturation Behavior in S_1/S_2. For S_1/S_2 excitation of TRP derivatives at 273 nm, the simplest scheme for the depletion of the ground state during the laser pulse is absorption followed by rapid picosecond order collision induced solvent relaxation to thermalized S_1/S_2 levels. In the absence of other processes (such as the photon-induced relaxation discussed above), the radiative and nonradiative $S_1/S_2 \rightarrow S_0$ relaxation rates should determine the population of ground-state molecules available for Raman scattering during the entire laser pulse. Thus, a simple model describing the saturation behavior is illustrated in Figure 9. P is the S_0 ground-state population at time t and σ_A is the absorption cross section (cm$^2/h\nu$) measured at 273 nm. $I(t) = I_0L(t)$ and describes the laser pulse intensity at time t; I_0 is the energy flux (mJ/cm^2) per pulse in the imaged sample volume. $L(t)$ is a normalized temporal pulse shape function. The state designated as P^* in Figure 9 represents all the S_1/S_2 fluorescing levels. K represents the sum of the rates of all radiative and nonradiative processes from S_1/S_2 to S_0. The curved arrow depicts the rapid collisional deactivation of the initially excited S_1/S_2 vibronic levels to thermalized S_1/S_2 levels at a rate K'. Under the photon fluxes considered here, K' is fast enough that absorption by the initially excited S_1/S_2 vibronic levels is completely negligible; we show below that absorption from *thermalized* S_1/S_2 levels is also negligible. The rate equation describing the ground-state population during the laser pulse is then

$$-\frac{d}{dt}P = \sigma_A I(t)P - KP^* \quad (1)$$

The total number of analyte molecules in the imaged sample volume is P_0. Since the excited-state lifetime associated with K' is ps, whereas the lifetime for excited states relaxing with the rate K is ns, P_0 is given at any time during the pulse by

$$P_0 = P + P^* \quad (2)$$

Substituting eq 2 into eq 1 and solving the rate equation for $P(t)$ yields

(31) Bazin, M.; Patterson, L. K.; Santus, R. *J. Phys. Chem.* **1983**, *87*, 189.
(32) Pigault, C.; Hasselman, C.; Laustriat, G. *J. Phys. Chem.* **1982**, *86*, 1755.

$$P(t) = \exp\left\{-\int_0^t (\sigma_A I(t) + K)\, dt\right\} \times \left[\int_0^t P_0 K \exp\left\{\int_0^t (\sigma_A I(t) + K)\, dt\right\} dt + C\right] \quad (3)$$

To proceed further, we require an explicit form of $I(t) = I_0 L(t)$. At present it is experimentally difficult to accurately specify I_0 within the illuminated sample volume. The sample absorption of ca. 0.3 causes the beam flux to decrease 2-fold through the sample thickness. I_0 for each volume element is therefore position dependent. Any variation in the efficiency of the collection optics for each volume element would also have to be considered, and an exact calculation of the saturation will require an appropriately weighted average of all the sample volume elements. At this stage we have prepared a sampling system as optically thin as possible and have focused the laser beam in such a way as to minimize the variation between different volume elements. To estimate I_0 for eq 3, we assume we collect light from all volume elements equally. We measure the energy flux over a ca. 0.15 × 0.60 mm area in the most intense portion of the beamspot at the front face of the sample. This 0.09-mm^2 area corresponds to the imaged area over which we can obtain maximum signal (±10%). This energy flux value is then corrected for the decrease in the beam intensity through the sample by utilizing the average energy flux through the sample thickness.

With I_0 defined in this manner, only the temporal pulse shape $L(t)$ in eq 3 needs to be considered further. The temporal pulse shape of our Nd:YAG laser system has an approximately Gaussian envelope with a fwhm of ca. 4 ns, but spiked and irregular fine structure exists within each pulse. This fine structure varies between pulses. However, we add the results of tens of thousands of laser pulses to average out the finer temporal features. We have examined both a Gaussian 4 ns fwhm pulse shape function as well as a simple "rectangular" function with a pulse period of 4 ns. We have used both temporal pulse shapes in our model to calculate the tryptophan derivative relaxation rates. These relaxation rates are accurately known from previous time-resolved fluorescence measurements. We obtain identical relative relaxation rates by using either pulse shape, but the absolute values differ by roughly 20% between these two pulse shapes if we utilize identical values of I_0. To obtain the correct known relaxation rates for the tryptophan derivatives, we can utilize either pulse shape and values of I_0 which are within 20% of the average I_0 value as calculated above. We do not as yet find a compelling reason to utilize the more realistic but numerically complex Gaussian temporal pulse shape function, since both pulse shapes give identical results within our uncertainties in estimating an effective average I_0 value. We therefore choose to use the simple rectangular pulse shape function since it results in a simple analytical expression for the relaxation rate dependent Raman intensity ratios described by eq 8 and eq 11 below.

$L(t)$ is thus taken as a function that has a value of $1/t_0$ for $0 < t < t_0$, where t_0 is the pulse period of 4 ns. $L(t)$ is then a normalized pulse shape function which when integrated over the laser pulse is equal to 1. In eq 3 we need only integrate over the interval $0 \le t \le t_0$ when the laser pulse is "on". In this case, $P(t = 0) = P_0$ and $C = P_0$ in eq 3, and it can be shown that by using the $L(t)$ just described, eq 3 becomes

$$P(t) = \frac{P_0}{\sigma_A I_0 + K t_0}\{K t_0 + \sigma_A I_0 \exp[-(\sigma_A I_0/t_0 + K)t]\} \quad (4)$$

The resonance Raman intensity observed for one laser pulse is

$$I_{RR} = \int_0^{t_0} \sigma_R I(t) P(t)\, dt \quad (5)$$

where σ_R is the Raman cross section of the analyte. Substituting eq 4 into eq 5 and integrating gives

$$I_{RR} = \frac{\sigma_R I_0 P_0}{(\sigma_A I_0 + K t_0)^2}\{(K t_0)^2 + \sigma_A I_0(1 + K t_0 - \exp[-(\sigma_A I_0 + K t_0)])\} \quad (6)$$

The Raman intensity of the non-absorbing internal intensity standard, I_S, will linearly increase with pulse energy flux because no depopulation of its ground state occurs during the laser pulse

$$I_S = \int_0^{t_0} \sigma_S I(t) C(t)\, dt = \sigma_S C_0 I_0 \quad (7)$$

where C_0 is the initial concentration of the internal standard and σ_S is the internal standard Raman cross section. The relative ratio of the analyte Raman intensity to the internal standard Raman intensity expected for one laser pulse is then just eq 6 divided by eq 7.

$$\frac{I_{RR}}{I_S} = \frac{\sigma_R P_0}{\sigma_S C_0 (\sigma_A I_0 + K t_0)^2}\{(K t_0)^2 + \sigma_A I_0(1 + K t_0 - \exp[-(\sigma_A I_0 + K t_0)])\} \quad (8)$$

Since the sample volume is regenerated between laser pulses, the integrated intensity observed is an average of many single pulse ratios described by eq 8. Also implicit in eq 8 is that σ_R does not change with increasing I_0. σ_R can be a function of I_0 if field strengths and dipole moments are large enough to produce Rabi frequencies high enough where vibrational and electronic population relaxation rates and T_2 dephasing relaxation rates begin to mix.[33-35] In this case the resonance Raman cross sections and line shapes begin to change. This phenomena has been invoked to explain the broadening of resonance Raman line shapes in β-carotene[36] and deoxy hemoglobin[37] at a pulse power flux of ca. 10^8 and 10^9 W/cm^2, respectively, in regions where molar absorptivities are ca. 10^5. We observe no spectral broadening in any data reported here. The highest pulse power flux data analyzed with eq 8 utilized power fluxes of ca. 7×10^6 W/cm^2 with molar absorptivities of 5×10^3.

The saturation scheme leading to eq 8 requires that each vibrational mode of a species will exhibit the same nonlinear behavior. Equation 8 predicts a smoothly decreasing intensity ratio with increasing I_0. Indeed, the observed S_1/S_2 saturation behaviors for the 1578 cm^{-1} TRP analogue bands in Figure 4 are well-described by eq 8. We can extract both σ_R and K by nonlinear least-squares fitting of eq 8 to the measured Raman saturation data. We experimentally determine the absorption cross sections (σ_A) at 273 nm. The values of $(1/K)$ obtained in this manner are given in column VI in Table I and are an average of the results of fitting both the 1578 and 1622 cm^{-1} band saturation behaviors over the flux range shown in Figure 4. Quoted errors are estimates of sample standard deviations. The values of $(1/K)$ derived for quenched NATA and TRPAM (pH 9) of 0.75 ± 0.07 and 7.2 ± 1.5 ns, respectively can be directly compared to the fluorescence lifetimes in column IV since the decays are single exponential. For the double exponential decays of TRPAM (pH 5) and TRP, we assume identical Raman cross sections for each decay component. In the case of TRP, for example, we then expect to obtain values of $(1/K)$ from the TRP Raman data corresponding to the best fit of eq 8 to a saturation response given by 22% of the molecules relaxing with a 0.62-ns lifetime and 78% with a 3.2-ns lifetime. These calculated values are given in column V of Table I. It is not possible, over the low flux ranges we utilize and with the current signal-to-noise ratios, for us to distinguish between two independent relaxation rates and the "single" lifetimes given in column V. The good agreement between columns IV and V and column VI in Table I indicates the following: (1) within the experimental error associated with measuring and defining I_0, our simple rectangular model for $L(t)$ provides adequate absolute agreements with fluorescence decay rates as well as relative agreements between different TRP derivatives, (2) the radiative and nonradiative $S_1/S_2 \rightarrow S_0$ relaxation rates dominate the relative

(33) Dick, B.; Hochstrasser, R. *Chem. Phys.* **1983**, *75*, 133.
(34) Dick, B.; Hochstrasser, R. *J. Chem. Phys.* **1984**, *81*, 2897.
(35) Deng, Z.; Mukamel, S. *J. Chem. Phys.* **1986**, *85*, 1738.
(36) Carrol, P. J.; Brus, L. E. *J. Chem. Phys.* **1987**, *86*, 6584.
(37) Alden, R. G.; Ondrias, M. R.; Courtney, S.; Findsen, E. W.; Friedman, J. M. *J. Phys. Chem.* **1990**, *94*, 85.

saturation behaviors, and (3) the triplet quantum yields must be relatively small and do not vary greatly between TRP derivatives. It should also be noted that least-squares fitting with eq 8 to give I_{RR}/I_S at zero laser flux provides a logical, quantitative method for determining Raman cross sections free from saturation artifacts. This will be discussed further below.

The photon-driven relaxation apparent at high-energy fluxes in Figure 3 must be avoided for eq 8 to be useful for deriving S_1/S_2 lifetimes. This photon-driven relaxation process derives from macroscopic properties; it is not a result of the field and the "isolated molecule" as was the power broadening in β-carotene and deoxy hemoglobin discussed above. This relaxation appears only at pulse energy fluxes where a S_1/S_2:S_0 population inversion occurs. Even at these higher fluxes, the incident photon flux is far too small to stimulate emission from the levels initially populated near 273 nm which survive only for ps. This suggests that the new photon-driven ground-state repopulation is amplified spontaneous emission (ASE) from the S_1/S_2 fluorescing levels. The spontaneous fluorescence could be radially amplified along the gain plane provided by the overlap of the ca. 1 mm excited beam spot and the 2.0 × 2.0 × 0.15 mm jet sample volume (the beampath is normal to the 2 × 2 mm jet plane). Our observation that shorter lifetime derivatives show a higher energy flux threshhold for the onset of the photon-driven process is consistent with an ASE process that requires a population inversion. In fact, comparing TRPAM (pH 9) with $K = (7\ \text{ns})^{-1}$ to that quenched with NaI with $K = (2.4\ \text{ns})^{-1}$ we see that the threshhold increases from ca. 30 to ca. 85 mJ/cm^2. The ratio of these pulse energy fluxes (ca. 3) is almost equal to the ratio of relaxation rates (7/2.4). We also measured the relaxed fluorescence intensity dependence upon energy flux and find that it drops off faster than does the Raman intensity at high energy fluxes; this is consistent with a directional ASE process.

S_3 Raman Saturation. In condensed phases internal conversion from higher excited electronic states to S_1 is generally considered to be fast (ps) and essentially 100% efficient. Normally, S_1 fluorescence quantum yields are found to be independent of excitation wavelength. Some notable exceptions to this general trend are phenol, tyrosine, indole derivatives, and tryptophan.[21,38,39] In the case of tryptophan, for example, although the fluorescence quantum yield throughout S_1/S_2 is constant, the quantum yield decreases by 30–50% with S_3 excitation.[24,25] The fluorescence quantum yield decrease has been shown to be accompanied by an increase of photoionization, which occurs rapidly enough to compete with internal conversion to the S_1/S_2 states (vide infra).

If we initially assume complete internal conversion from S_3 to S_1/S_2 for all the TRP analogues studied here, the model for saturation behavior in S_3 is identical with that depicted in Figure 9 except that the initial excitation is into S_3 which rapidly relaxes to P* (S_1/S_2). Equation 8 then describes the expected saturation behavior and values of $(1/K)$ derived in S_3 should be similar to those derived in S_1/S_2. We use the measured absorption cross sections at 225 nm and utilize the rectangular pulse shape described previously. The least-squares best fits of eq 8 to the 1555-cm^{-1} data below ca. 15 mJ/cm^2 are shown in Figures 6–8 by the solid curves. We obtain good relative and absolute agreements to the fluorescence decay components for NATA, NATE, and TRPAM (pH 9) (see column VII, Table I). The values of $(1/K)$ listed in column VII are averages of the values obtained by fitting the 760-, 1015-, and 1555-cm^{-1} bands of each compound separately. Errors quoted are estimated standard deviations. The values of $(1/K)$ of 2.9 ± 0.5, 1.3 ± 0.2, and 7.1 ± 1.5 ns for NATA, NATE, and TRPAM (pH 9) are essentially identical with their S_1/S_2 fluorescence lifetimes, which indicates similar internal conversion efficiencies for these three compounds. Thus, the S_3 saturation is determined by the radiative and nonradiative $S_1/S_2 \rightarrow S_0$ relaxation rates as observed with S_1/S_2 excitation at 273 nm. In contrast, the solid curves modeled by eq 8 shown in Figures 6 and 8 for TRPAM (pH 5) and TRP result in significantly longer $(1/K)$ lifetimes than their S_1/S_2 lifetimes (column VII). This suggests that for TRP and TRPAM (pH 5) for excitation in S_3 an additional process competes effectively with internal conversion to S_1/S_2 and leads to a state or states that are long lived compared in our laser pulse length. For comparison, the expected saturation behavior for TRP based on the TRP S_1/S_2 lifetime is shown by the dashed curve in Figure 8.

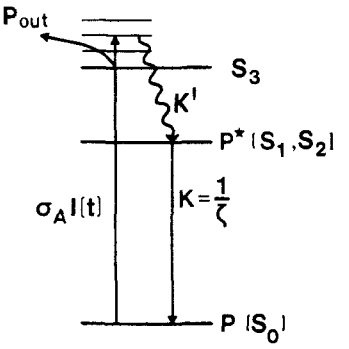

Figure 10. Model for Raman saturation for excitation in S_3 at 225 nm. See text for details.

To estimate the fractional number of species that do not convert from S_3 to S_1/S_2 for TRP and TRPAM (pH 5), we utilize a saturation model shown in Figure 10 where all parameters are as defined in Figure 9. P_{out} represents states derived directly from S_3 excitation, which are long lived relative to our 4-ns laser pulse. P_{out} in Figure 10 is populated prior to internal conversion to S_1/S_2 with a quantum yield of ϕ_{out}. This phenomenologically models, for example, monophotonic photoionization from S_3, which could compete with internal conversion to give long-lived radical species. The rate equations for the model in Figure 10 are given by eq 1 and eq 9.

$$\frac{d}{dt}P_{out} = \phi_{out}\sigma_A I(t)P \tag{9}$$

The total number of molecules in the imaged sample volume is P_0 and is given at any time during the laser pulse as

$$P_0 = P + P^* + P_{out} \tag{10}$$

It is shown in the Appendix that the pulse energy flux dependence of the analyte to internal standard Raman intensity ratio for the saturation model of Figure 10 is

$$\frac{I_{RR}}{I_S} = \frac{\sigma_R P_0}{\sigma_s C_0}\left\{\frac{1}{\phi_{out}\sigma_A I_0} + \frac{(2\phi_{out}\sigma_A I_0 - Kt_0 - \sigma_A I_0 - F^{1/2})\exp[\tfrac{1}{2}\{-(Kt_0 + \sigma_A I_0) + F^{1/2}\}]}{2\phi_{out}\sigma_A I_0 F^{1/2}} - \frac{(2\phi_{out}\sigma_A I_0 - Kt_0 - \sigma_A I_0 + F^{1/2})\exp[\tfrac{1}{2}\{-(Kt_0 + \sigma_A I_0) - F^{1/2}\}]}{2\phi_{out}\sigma_A I_0 F^{1/2}}\right\} \tag{11}$$

where $F = (Kt_0 + \sigma_A I_0)^2 - 4\phi_{out}Kt_0\sigma_A I_0$. We can determine ϕ_{out} for TRP and TRPAM (pH 5) by using eq 11 with the values of $(1/K)$ that we obtained with S_1/S_2 excitation for these compounds (or we can use the measured values of $(1/K)$ based on the S_1/S_2 fluorescence lifetime data). The least-squares fit extracts σ_R and ϕ_{out}. For TRP, we find that $\phi_{out} \cong 80\%$, while for TRPAM (pH 5) $\phi_{out} \cong 55\%$; these fits give essentially identical solid curves as those in Figures 6 and 8.

Equations 11 and 8 can be used to derive accurate resonance Raman cross sections for S_3 excitation where the saturation is particularly severe. For example, the fit of the relative intensity ratio I_{RR}/I_S below 15 mJ/cm^2, extrapolated to zero pulse energy flux, gives at 225-nm excitation Raman cross sections of 2.2, 1.4, and 1.8 barns/(molecule·steradian) for the 1555-, 1015-, and 760-cm^{-1} bands of TRP. These values are 2 to 3 times larger than those recently reported by Fodor et al.[40] for TRP at 225 nm. Fodor

(38) For reviews, see: Creed, D. *Photochem. Photobiol.* **1984**, *39*, 563.
(39) Creed, D. *Photochem. Photobiol.* **1984**, *39*, 576.

et al. claimed that the ratio of the TRP bands to the nonabsorbing sulfate internal standard bands was constant over the pulse energy range utilized. However, only one data point below ca. 90 mJ/cm^2 was obtained. Figure 8 demonstrates a 2-fold change in the TRP/internal standard intensity ratios occurs between 0 and 15 mJ/cm^2 pulse energy flux. This clearly shows that the data of Fodor et al. were measured in an energy flux regime where ASE relaxation processes discussed above lead to a very weak dependence of TRP/internal standard intensity ratios upon I_0. This also explains why their relative intensity ratios are 2- to 3-fold smaller than our values.

Origin of ϕ_{out} Differences between TRP Derivatives in S_3. Our ability to quantitatively determine ϕ_{out} is limited both by the signal-to-noise ratios of the data and by the error associated with specifying I_0 and $L(t)$. Thus, we estimate that although we find ϕ_{out} values of ca. "zero" for S_3 excitation of NATA, NATE, and TRPAM (pH 9), our uncertainties could permit ϕ_{out} values as large as ca. 20%. The central point is, however, that we obtain a ϕ_{out} value considerably larger for TRP and TRPAM (pH 5). To ensure that these variations in ϕ_{out} did not derive from sequential two-photon absorption where photoionization occurs by S_1/S_2 excited-state absorption, we studied the saturation behavior of TRP at pH 1.3 (where the carboxylate group is protonated). Protonation of the carboxylate group leads to a large decrease in the S_1/S_2 lifetime due to enhanced charge-transfer quenching;[17] we measure an 8-fold fluorescence intensity decrease. The shorter S_1/S_2 lifetime must result in a decreased S_1/S_2 absorption probability. Equation 11 was fit to our data, which were obtained between 0 and 15 mJ/cm^2 energy fluxes. Utilizing the appropriate value of $(1/K)$ for S_1/S_2 relaxation, we obtain a similar ϕ_{out} = 70% value for TRP (pH 1.3) excited at 225 nm.

Our S_3 resonance Raman saturation results, which indicate large ϕ_{out} values for TRP and TRPAM (pH 5), are qualitatively consistent with the few other relevant studies of S_3 photophysics of TRP derivatives. As discussed above, the S_1/S_2 fluorescence quantum yields of a few indole derivatives as well as TRP decrease with excitation in S_3. Steen et al.[24] measured a decrease of 30% in the S_1/S_2 quantum yield of TRP between 260 and 230 nm while Tatischeff and Klein[25] measured a 50% decrease over the same region. It was demonstrated that this decrease does not derive from a change in the intersystem crossing rate.[24] In this same spectral region, several workers observed dramatic increases in electron ejection (photoionization) quantum yields (ϕ_e), although the absolute values are not all in agreement. For TRP, Steen et al. find at 220 nm ϕ_e = 15–20%, while Amouyal et al.[23] find ϕ_e larger than 50% even at 240 nm, the short wavelength limit of their experiment. Considerable data support the idea that a "charge transfer to solvent state" occurs sufficiently rapidly from initially excited S_3 vibronic levels to compete with internal conversion to S_1/S_2.[26-28] Electron release to solvent from the "charge transfer to solvent state" is thermally activated and may compete with direct back-reaction relaxation to the ground state of the indole. The radical species formed after electron release have microsecond lifetimes[41-43] and are likely to dominate our ϕ_{out} values. The lack of appearance of new Raman bands due to the photoionized or even S_1/S_2 excited-state species is primarily due to our low-energy fluxes. At higher laser powers with 235-nm excitation, for example, we observe new bands.[12]

Our observation of much larger ϕ_{out} values for TRP and TRPAM (pH 5) than for NATA, NATE, and TRPAM (pH 9) is novel. To our knowledge fluorescence quantum yields and electron ejection quantum yields in S_3 are unknown for any of the compounds studied here except TRP. In common with S_1/S_2 excitation studies,[39] we find that the S_3 excited-state photophysics is influenced by the identity of the R and R′ groups. The fact that TRP and TRPAM (pH 5) have large ϕ_{out} values suggests that the protonated amino group promotes electron ejection. The NH_3^+ group must either assist the initial formation of the charge transfer to solvent state or influence the yield of electron release. An electrostatic field effect of the protonated amino group on the indole nucleus, facilitating initial electron ejection, was postulated previously for S_1/S_2 excitation.[44,45] Although the work here does not conclusively determine the identity of the long-lived transient species, it demonstrates its existence through the observed saturation phenomenon. In the future we will attempt to resonance enhance these transient species to uniquely identify them, in a manner similar to our previous study which identified the formation of tyrosyl radical with excitation at 220 nm in tyrosine and at 245 nm in tyrosinate.[12,14]

UV Resonance Raman Saturation Spectroscopy. The quantitative relationships demonstrated here between the UV Raman saturation behavior and $S_3 \rightarrow S_1/S_2$ internal conversion efficiencies and S_1/S_2 lifetimes indicate that the UV resonance Raman saturation spectroscopy may be useful as a methodology for monitoring photophysical relaxation processes in complex systems and environments. Although time-resolved fluorescence techniques also give essentially identical information, the UV Raman saturation methodology has the advantage of vibrational resolution. The wavelength dependence of the resonance Raman effect and the vibrational resolution of the Raman spectra make it possible to resolve saturation of a single Raman band of a particular chromophore. It is obviously difficult to resolve between the broad overlapping fluorescence bands of condensed phase aromatic species. Another advantage is that, unlike time-resolved fluorescence techniques, where the detector response time determines the possible temporal resolution (in the pico- and femtosecond time scales), the time scales that can be probed by the UV saturation method are, in principle, limited only by the energy flux of the laser pulse. In principle, any photon counting device will serve as a detector. It should be noted, however, that the optimal laser pulse length for ps and fs relaxation studies probably would be in the ps and fs time regime. Study of these fast relaxations with ns pulse lengths would require high pulse powers, which could lead to higher order nonlinear processes that would complicate the measurements.

Raman saturation spectroscopy at present suffers from a lower sensitivity than time-resolved fluorescence due to the signal-to-noise ratios presently available. Thus, time-resolved fluorescence techniques will be superior for determining multiexponential decays, or if highly accurate decay rates are required. However, the two techniques are highly complimentary. Fluorescence techniques monitor excited-state depletion while the UV Raman saturation technique reports directly on ground-state recovery. Fluorescence techniques are dominated by those chromophores with the largest fluorescence quantum yields, while the UV Raman saturation method is equally sensitive to species with large or zero fluorescence quantum yields.

We envision a number of applications of UV Raman saturation spectroscopy. Of particular interest to our laboratory is utilizing this saturation methodology to determine tyrosine, phenylalanine, as well as tryptophan residue excited state relaxation rates in order to monitor protein structure and conformational changes. The difficulties in applying fluorescence techniques, such as the low fluorescence quantum yields of phe and tyr in proteins, have already been discussed. Other ground-state recovery techniques, such as measuring the laser flux dependence of the optical density, would also be extremely difficult due to the overlap of aromatic amino acid and amide group absorption spectra in typical proteins. The UV Raman saturation methodology has promise since at least one vibrational mode of each aromatic amino acid can be completely resolved without interference from other aromatic residues or amide vibrations with excitation in the 240–195 nm spectral region. From the work reported here, we anticipate that the Raman saturation methodology will be sensitive enough to detect

(40) Fodor, P. A.; Copeland, R. A.; Grygon, C. A.; Spiro, T. G. *J. Am. Chem. Soc.* **1989**, *111*, 5509.
(41) Bent, D. V.; Hayon, E. *J. Am. Chem. Soc.* **1975**, *97*, 2612.
(42) Baugher, J. F.; Grossweiner, L. I. *J. Phys. Chem.* **1977**, *81*, 1349.
(43) Volkert, W. A.; Kuntz, R. R.; Ghiron, C. A.; Evans, R. F.; Santas, R.; Bazin, M. *Photochem. Photobiol.* **1977**, *11*, 227.
(44) Fleming, G. R.; Morris, J. M.; Robbins, R. J.; Woolfe, G. J.; Thistlewaite, P. J.; Robinson, G. W. *Proc. Natl. Acad. Sci. U.S.A.* **1978**, *75*, 4652.
(45) Werner, T. C.; Forster, L. S. *Photochem. Photobiol.* **1979**, *29*, 905.

interactions with nearby residues that alter the major decay components or which influence photochemistry. We will show in a subsequent report that Förster energy transfer strongly influences the UV resonance Raman saturation behavior of aromatic amino acids in a number of peptides and proteins.

Conclusions

We have derived expressions to extract ground-state recovery rates from resonance Raman saturation behaviors of a number of tryptophan derivatives. These recovery rates agree well with excited-state decay rates as determined by fluorescence techniques. Decreases in the relative $S_3 \rightarrow S_2/S_1$ internal conversion efficiencies for several tryptophan derivatives have been observed that appear to be related to the presence of a protonated amino group near the indole ring. We suggest these differences derive from a greater degree of monophotonic photoionization upon S_3 excitation. The quantitative success of these Raman saturation studies suggests that UV resonance Raman saturation spectroscopy is a new methodology that will be useful for studying photophysical relaxation processes. This technique is complementary to time-resolved fluorescence techniques since it reports directly on ground-state recovery rates. The Raman saturation technique has the advantage of vibrational resolution, as chromophore-specific relaxation rates can be probed by vibrational markers. The UV Raman saturation methodology will be particularly useful in monitoring phenylalanine and tyrosine, as well as tryptophan residue relaxations in proteins and other biological molecules.

Acknowledgment. We gratefully acknowledge support of this work from NIH Grant 1R01GM37041-08. Sanford A. Asher is an Established Investigator of the American Heart Association. This work was done during the tenure of an Established Investigatorship of the American Heart Association, Pennsylvania affiliate.

Appendix

We show here the derivation of eq 11. Substitution of eq 1 into eq 10 gives

$$-\frac{dP}{dt} = (\sigma_A I(t) + K)P - KP_0 + KP_{out} \tag{12}$$

Equation 9 is rearranged to

$$P = \frac{1}{\sigma_A I(t)\phi_{out}} \frac{d}{dt} P_{out} \tag{13}$$

Equation 13 is substituted for P into eq 12 yielding

$$\frac{d^2}{dt^2} P_{out} + (\sigma_A I(t) + K) \frac{d}{dt} P_{out} + (K\phi_{out}\sigma_A I(t))P_{out} = K\phi_{out}\sigma_A I(t)P_0 \tag{14}$$

Solving this differential equation for P_{out}

$$P_{out} = C_3 \exp(\alpha t) + C_2 \exp(\beta t) + C_1$$

where C_1, C_2, and C_3 are to be determined from the boundary conditions and α and β are

$$\alpha = \tfrac{1}{2}\{-A + A^2 - 4B\}$$

$$\beta = \tfrac{1}{2}\{-A - A^2 - 4B\}$$

where

$$A = \sigma_A I(t) + K$$

$$B = K\phi_{out}\sigma_A I(t)$$

Using the initial condition for $P_{out}(t = 0) = 0$ and eq 13 and with the initial condition for $P(t = 0) = P_0$ yields

$$P(t) = \frac{P_0}{\beta - \alpha}\{(K + \beta) \exp(\beta t) - (K + \alpha) \exp(\alpha t)\} \tag{15}$$

which, for $\phi_{out} = 0$, is identical with eq 4 since $\sigma_A I(t) = (\sigma_A I_0)/t_0$. The expression for $P(t)$ of eq 15 is substituted into eq 5 and integrated from 0 to t_0 to give

$$I_{RR} = \frac{\sigma_R P_0 I_0}{t_0}\left\{\frac{K + \beta}{\beta(\beta - \alpha)} \exp(\beta t_0) - \frac{K + \alpha}{\alpha(\beta - \alpha)} \exp(\alpha t_0) + \frac{K}{\alpha\beta}\right\} \tag{16}$$

Equation 16 divided by eq 7 gives I_{RR}/I_S, yielding eq 11.

Registry No. TRP, 73-22-3; NATA, 2382-79-8; TRPAM, 20696-57-5; NATE, 2382-80-1.